Supporting Information

Earth's field NMR relaxation of pre-polarised water protons for real-time detection of free-radical formation

Table of contents:

I. Experimental NMR apparatus and methods for the determination of relaxation time constants in Earth's magnetic field

I.1 Apparatus

The Earth-field NMR apparatus used for our experiments was developed by Terranova MRI. It is designed to conduct NMR relaxation and imaging experiments and it consists of a three-component probe system and an ultra-low frequency spectrometer (Fig. S1). The three-component probe includes a polarizing coil, an excitation/detection coil and a gradient coil set.

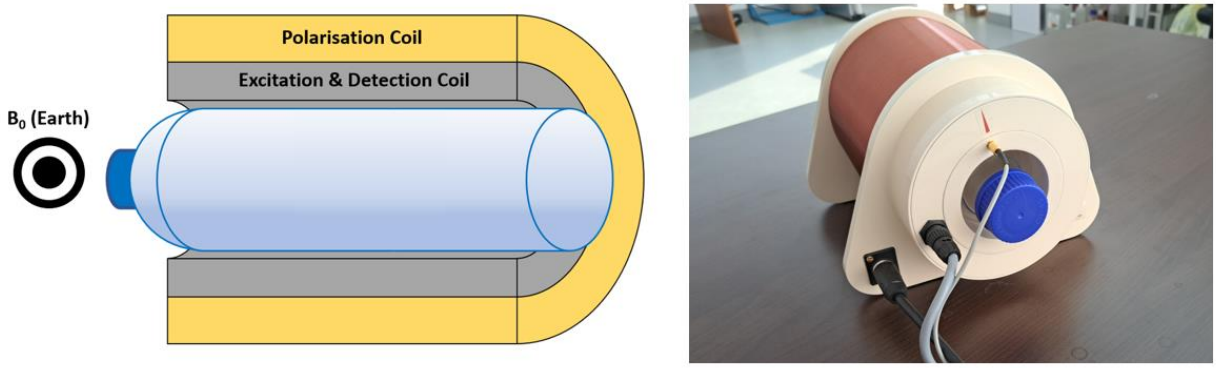

Fig. S1. The experimental setup: Terranova MRI system and chemical reaction monitoring in aqueous samples.

For magnetisation excitation and detection, a solenoid tuned by the resonance circuitry to the water ^{1}H Larmor frequency corresponding to Earth's field - $\nu_0(^1\mathrm{H})$ = 2.3 kHz at our location - is used. A set of gradient coils is provided for multi-dimensional imaging and for shimming.

An additional polarizing coil is used to boost the thermal magnetisation of the sample before excitation and free-precession in the Earth's field (B_{Earth} = 0.05 mT at our location), and therefore to enhance the sensitivity of the method. The polarizing coil is solenoidal and produces a magnetic field B_{p} =18.7 mT along its axis when a 6 A current is used. The inhomogeneity of this field is at most 10 - 15% within a cylindrical region of 100 mm in length and 75 mm in diameter.

I.2 Pulse sequences

The pulse sequences employed for the measurement of longitudinal and transverse relaxation rate constants as a function of free-radical concentration are variants of classical methods: (i) perturbation of initial magnetisation followed by longitudinal relaxation to its equilibrium value and (ii) series of time-points of transverse magnetisation evolution while the chemical shift evolution is refocused. We have improved sensitivity for NMR experiments in Earth's magnetic field without altering the specific precession frequency via pre-polarisation: a polarising magnetic field, perpendicular to the Earth's field, was generated in the first experimental step (Figs. S2-S3).

Once polarisation has built-up using a current I_p in the enhanced magnetisation (or polarisation), the pre-polarising field is switched off and the polarisation is adiabatically converted to the Earth's magnetic field orientation, and decays back to its equilibrium value.

$$M_0 \sim \frac{N_s \gamma^2 \hbar^2 (B_p/I)}{4 k_B T} I_p \sim \varepsilon M_{Earth}$$

In the equation above, M_0 is the magnetisation/polarisation after applying a polarising current I_p to saturation (typically 6 seconds), B_p is the characteristic field of the polarising coil for a unit current I, N_S is the natural population of polarised spins in Earth's field, γ is the proton gyromagnetic ratio, $\hbar$ is the Planck constant, k_B is Boltzmann's constant and T is the sample temperature. The enhancement factor obtained by pre-polarisation is $\varepsilon = B_p/B_{Earth} \sim 350$.

The pulse sequences used to determine the longitudinal and transverse NMR relaxation parameters, T_1 and T_2, are tailored to the conditions of adiabatic switching off of the polarizing field followed by the excitation and detection in Earth's field.

(i) Longitudinal relaxation of magnetisation: the polarisation-recovery experiment

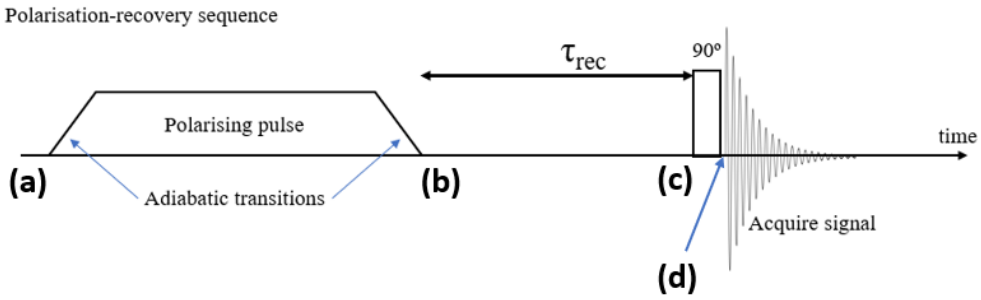

Fig. S2. Polarisation-recovery sequence with highlighted time points of magnetisation evolution

The initial magnetisation arising purely from Earth's field (a) is subjected to a polarising pulse then adiabatically led towards a parallel orientation with respect to the Earth's magnetic field (b). Polarisation-enhanced magnetisation M_0 decays under the action of longitudinal relaxation during various evolution time points τ_{rec} as $M_{//}(\tau_{rec})$. At the end of this time, the $M_{//}$ magnetization remaining (c) is flipped by a 90° pulse to transverse magnetisation M_t in order to produce a signal in the measuring coil (Fig. S2).

The characteristic longitudinal relaxation time constant T_1 is obtained by plotting the obtained signal with respect to τ_{rec} according to the equations below:

Time point (b): $M_{//}(0) = M_0$

Time point (c):

$$M_{//}(\tau_{rec}) = M_0[1 - \exp\left(\frac{-\tau_{rec}}{T_1}\right)]$$

Time point (d):

$$M_{//}(\tau_{rec}) \rightarrow M_t(\tau_{rec})$$

(ii) Transverse relaxation of magnetisation: the Carr-Purcell-Meiboom-Gill (CPMG) experiment

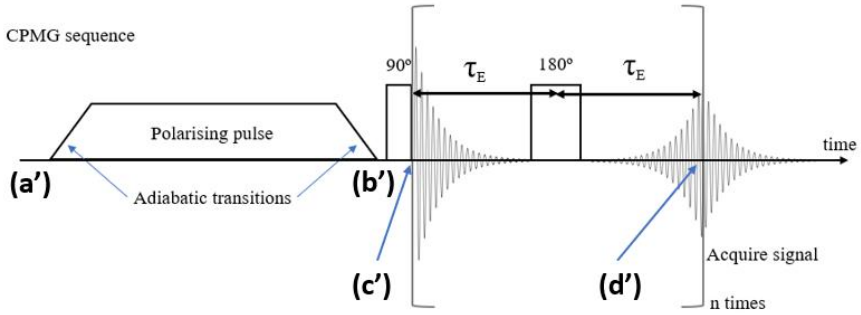

Fig. S3. CPMG sequence and time points of magnetisation evolution

The transverse relaxation time, T_2, is determined from the decay of the echo-train generated by the **Carr-Purcell-Meiboom-Gill (CPMG)** method (Fig. S3). The sequence consists of a suite of 180° pulses designed to refocus the chemical shift evolution. The pulses are equidistantly applied to generate additional echoes, starting from an initial 90°-180° spin-echo.

The initial magnetisation arising purely from Earth's field (a'), is subjected to a polarising pulse and adiabatically switched to Earth's field orientation (b'). Magnetisation M_0 is flipped by a 90º pulse and becomes transverse $M_t(0)$ at point (c'). This magnetisation evolves by precessing around Earth's field. The 90º-180º delay is defined as τ_E, at this point the 180º pulse flips the M_t magnetisation to -M_t, after another delay of τ_E the magnetization M_t is refocused and the spin echo produces a signal. Thus, increasing steps of $2\tau_E$ (echo times) refocus the signal and allow for repeated measurements (d'), plotting the signal versus the $2\tau_E$ steps yields the relaxation time constant T_2, according to the equations below:

Time point (b'): $M_{//}(0) = M_0$

Time point (c'): $M_{//}(0) \rightarrow M_t(0)$

Time point (d'): $$M_t(2\tau_E) = M_t(0) \exp\left(\frac{-2\tau_E}{T_2}\right)$$

Table S1. Parameters used in our EFNMR experiments

Longitudinal Relaxation (polarisation-recovery)	90º pulse duration (ms)	Pre-90º delay step size (ms)	No. of steps	90º Acquisition delay (ms)	No. of data points	Acquisition time (s)	Repetition time (s)	No. of scans
	1.3	500	15	25	16384	1	20	1

Transverse Relaxation (CPMG)	Concentration (timeframe) regime	90º pulse duration (ms)	180º pulse duration (ms)	No. of Echoes	Echo time (ms)	No. of data points	Dwell time (µs)	No. of scans
	Low conc.	1.3	2.7	30	100	1024	100	8
	High conc. (stable paramagnets)			20	35		20	4
	High conc. (oxygen production)			15	50	256	50	

More details of the methods implementation Terranova Earth's field equipment can be found in the main text Reference 3 and the following link: http://researcharchive.vuw.ac.nz/handle/10063/1198.

I.3 Sample preparation

In the case of stable paramagnets, each measurement was carried out in a 315 mL flask by preparing a sample of the relaxation agent in de-ionised water, at concentrations ranging from 1 mM down to 3.9 µM by successive dilutions. A pure water sample was used as reference when performing polarisation-recovery experiments to determine T_1 or CPMG sequences to determine T_2. The obtained T_1 and T_2 values were converted to relaxation rate constants $R_1 = 1/T_1$ and $R_2 = 1/T_2$ in order to describe water ^{1}H magnetisation relaxation as a linearly-dependent quantity on the concentration of the paramagnetic compound.

For the free-radical generation experiments, after preparation in a 315 mL flask with known starting concentrations of H_2O_2 and CsI as the catalyst, all samples were quickly introduced in the Earth-field NMR magnet detection coil and CPMG measurements were performed at set intervals until T_2 reached a plateau. The relaxation rate constant $R_2 = 1/T_2$ dependence on the reaction time was used to follow the reaction evolution. In the case of the first reaction pathway – described by eqns. (1)-(2) in the main text, without a spin-trap molecule - multiple sets of experiments were performed with different starting concentrations to test the response of the chemical system and to gain information about the regime in which the reaction order changes for either species. When using 5 mM H_2O_2 and 50 mM CsI, the reaction is 0^{th}-order with respect to the catalyst and 1^{st}-order with respect to the reactant. We used these starting conditions to fit the kinetic model via the relaxation rate constant values (R_2), which increase with the concentration of produced O_2. For the second pathway, which takes place in the presence of a spin-trap and is described by Eqns. (1)-(3) in the text, a similar experiment was conducted using PBN to trap ·OH radicals, with the starting concentrations being 5 mM H_2O_2, 50 mM CsI, and 20 mM PBN.

I.4 Fits of experimental data

For paramagnetic relaxation rate constant determination experiments with stable free-radicals as the relaxation source, examples of T_1 and T_2 measurements are shown in Fig. S4. The low-concentration domain of the relaxation rate constants $R = 1/T$ is shown in Fig. S5; relaxivity values are listed in Table S2.

Fig. S4. Examples of fits of T_1 (left) and T_2 (right) for TEMPO solutions of 1 mM (top), 0.125 mM (middle) and

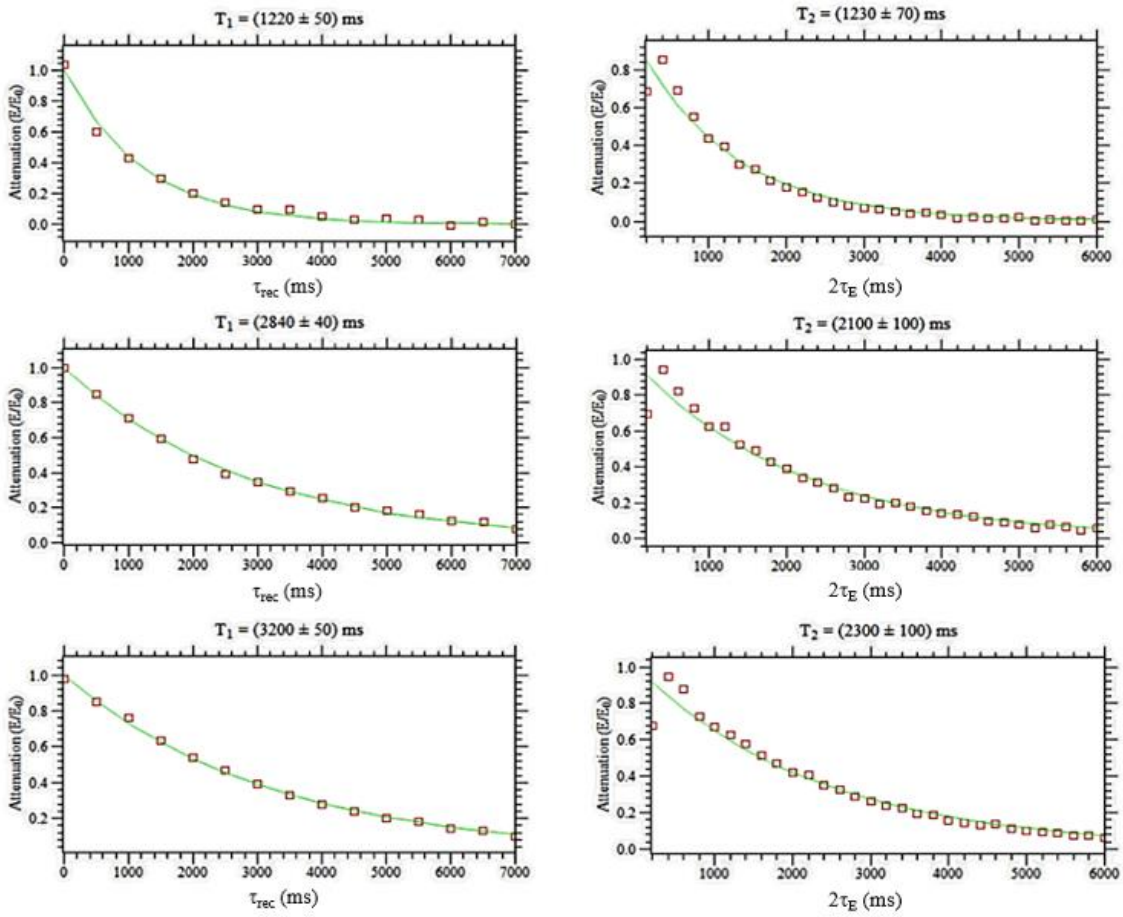

0.031 mM (bottom). Amplitude data is plotted versus recovery time (τ_E) for T_1 and versus echo time ($2\tau_E$) for T_2.

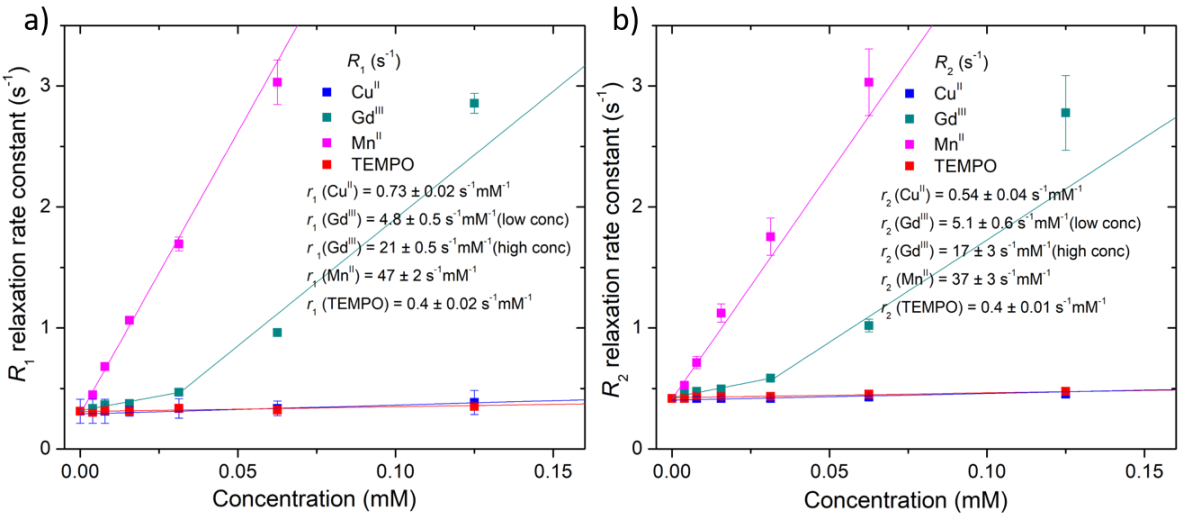

Fig. S5. Plots of R_1 (a) and R_2 (b) in the low-concentration region; Gd^{III} features two linear relaxation regimes, possibly indicating a change in dominant electronic relaxation dynamics due to inter-ion interactions above 50 µM concentration.

Table S2. Longitudinal and transverse NMR relaxivity values in water solution.

Species	**r_1 (s^{-1} mM^{-1})**	**r_2 (s^{-1} mM^{-1})**
TEMPO	0.40 ± 0.02	0.40 ± 0.01
Cu^{II}	0.73 ± 0.02	0.54 ± 0.04
Gd^{III}	4.8 ± 0.5	5.1 ± 0.5
	21.0 ± 0.4	16.9 ± 2.8
Mn^{II}	46.6 ± 2.4	37.4 ± 3.2

The relaxivity values obtained for transition metal ions warrant detection of changes in paramagnetic relaxation effects upon changes in concentration in the range of tens of micromolar. In the case of organic free radicals, changes in concentration in the mM range are needed in order to induce observable effects.

II. Reproducibility and error analysis for hydrogen peroxide decay results, kinetic model

II.1 Reproducibility, error analysis

The reproducibility of the experimental data for the radical-generation experiments was tested recording three data sets in the same conditions (fig. S5). The error ranges and average errors for all experiments are listed in Table S3.

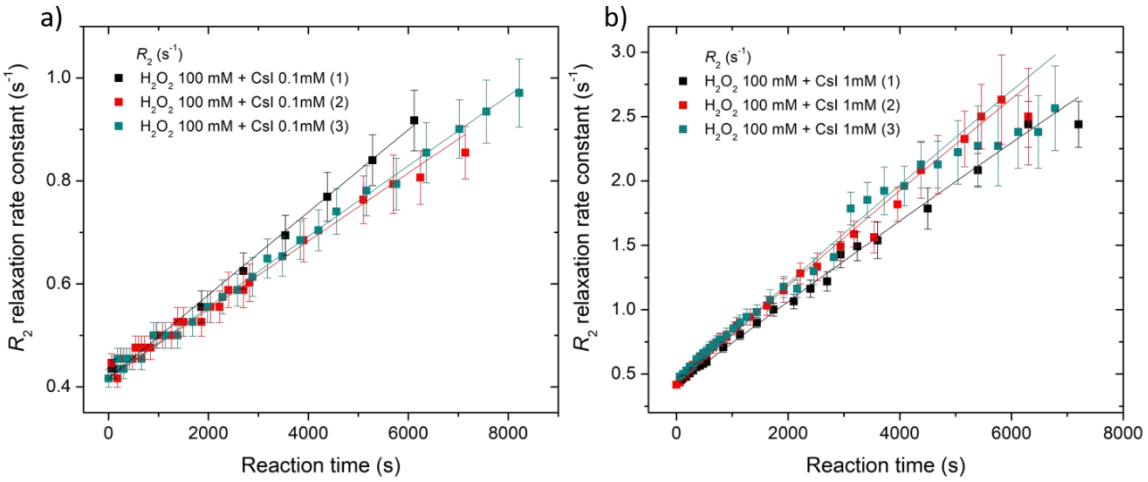

Fig. S6. H_2O_2 decay reproducibility with 100 mM H_2O_2 starting concentration and 0.1 mM (a), 1 mM CsI (b) concentration.

Relaxation rate constants recorded for solutions containing only H_2O_2 (no catalyst) or only the CsI (no H_2O_2) were within the standard deviation of relaxation rates recorded for samples without any reactant both in the case of water samples and in the case of cell-growth media (see below).

Table S3. Error data for H_2O_2 decay experiments

H_2O_2 decay experiments error data							
H_2O_2 conc.	CsI conc.	Spin-trap (PBN) conc.	Cell growth medium	R_2 Error range (s^{-1})	R_2 Mean Error (s^{-1})	R_2 Median Error (s^{-1})	Standard Deviation of errors (s^{-1})
100 mM	-	-	-	0.017 - 0.035	0.02	0.0198	0.005
100 mM	0.1 mM	-	-	0.017 - 0.065	0.032	0.028	0.013
100 mM	1 mM	-	-	0.017 - 0.381	0.097	0.057	0.088
100 mM	5 mM	-	-	0.017 - 0.781	0.200	0.148	0.174
100 mM	10 mM	-	-	0.017 - 1.171	0.310	0.185	0.274
10 mM	10 mM	-	-	0.017 - 0.140	0.061	0.058	0.030
1 mM	10 mM	-	-	0.017 - 0.039	0.025	0.022	0.006
5 mM	50 mM	-	-	0.003 - 0.048	0.019	0.017	0.009
5 mM	50 mM	20 mM	-	0.006 - 0.031	0.016	0.016	0.005
100 mM	10 mM	-	present	0.028 - 2.221	0.420	0.259	0.631

Kinetic model fit parameters for the pseudo-1st order reaction							
H_2O_2 concentration	CsI concentration	Spin-trap (PBN) concentration	k_{decay} (s^{-1})	Error in k_{decay} (s^{-1})	Conversion factor α	Error in α	R^2 coefficient
5 mM	50 mM	No PBN	$1.38 \cdot 10^{-3}$	$0.04 \cdot 10^{-3}$	-	-	0.996
5 mM	50 mM	20 mM	$1.63 \cdot 10^{-3}$	$0.04 \cdot 10^{-3}$	0.103	0.007	0.997

Reference solutions for all catalysed decay experiments contain only the catalyst, the measured R_2 is always the t=0 point in these experiments. The determination coefficient R^2 is defined as the ratio of the regression sum of squares over the total sum of squares. Error bars in relaxation rate / time constants are given as standard deviations of parameters from the fits of water ^1H intensities as a function of time delays (fig. S4).

II.2 Kinetic model

The global chemical reaction's kinetics can be represented by:

$$H_2O_2 \xrightarrow{k_{decay}} \frac{1}{2} O_2 + H_2O$$

with starting concentrations: $[H_2O_2]_0 \quad [O_2]_0 = 0$

and concentrations at time t: $[H_2O_2](t) = [H_2O_2]_0 - x(t); \quad [O_2](t) = \frac{1}{2} x(t)$

Herein, $[H_2O]$ is considered a constant, as any changes are very small compared to the bulk, x is a conversion factor, CsI catalyst is not included in the global model, as its concentration (50 mM) is 10 times larger than that of H_2O_2 (5 mM). We consider the conditions pseudo-0th-order relative to the catalyst, since its net action is included in the global kinetic constant k_{decay}, and pseudo-1st-order relative to the reactant, H_2O_2.

This simplified approach is only valid for the data fits in Fig. 4 of the main text.

The basic rate law:

$$v(t) = \frac{-d[H_2O_2](t)}{dt} = k_{decay}[H_2O_2](t)$$

yields, integrating for time and concentration ranges and expressing oxygen evolution:

$$[O_2](t) = \frac{1}{2}[H_2O_2]_0(1 - e^{-k_{decay}t})$$

Taking into account the relaxivity of oxygen, $r_2(O_2)$, and the fact that the measured solution relaxation rate constant R_2 is the sum of the reference $R_{2initial}$ (measured on a reference solution of 50 mM CsI) and the additional relaxation contribution due to oxygen production $R_2(O_2)(t)$, the rate law for the global reaction is:

$$R_2(t) = R_{2initial} + R_2(O_2)(t); \quad R_2(O_2)(t) = [O_2](t) \cdot r_2(O_2)$$

$$R_2(t) = R_{2initial} + \frac{r_2(O_2)}{2}[H_2O_2]_0\left(1 - e^{-k_{decay}t}\right)$$

The addition of spin-traps perturbs the system, and the conversion factor α accounts for this perturbation occurring via the competition of PBN for ·OH radicals against the recombination of ·OH radicals to yield O_2. In this case:

$$R_2(t) = R_{2_{initial}} + (1 - \alpha)\frac{r_2(O_2)}{2}[H_2O_2]_0\left(1 - e^{-k_{decay}t}\right)$$

III. Relaxation rate constants for free radical detection in cell-growth medium

We used Earth-field NMR to monitor paramagnetic species formation in cell-growth DMEM medium taken from a glioblastoma cell culture sample. The cell growth's medium initial composition consists of amino-acids and metabolites (DMEM high-glucose with calf serum W/L-Glutamine W/o Sodium Pyruvate, EU Cat No. 392-0414) treated with ampiciline and streptomicine: https://si.vwr.com/assetsvc/asset/sl_SI/id/36648559/contents/tds-dmem-with-4-5-g-per-l-glucose-with-l-glutamine-without-sodium-pyruvate-500-ml_392-0414.pdf

The medium was collected one week after cell culture initiation in order to ensure the presence of products of cell catabolism. The medium was then stored at -80º C prior to Earth's field NMR measurements. The stability of the cell-growth medium after warming to room temperature in absence of any H_2O_2 or catalyst was checked by ^1H NMR relaxation profiles shown in Fig. S7 (a). The effects of adding 100 mM H_2O_2 and monitoring of the medium response are shown in Fig. S7 (b).

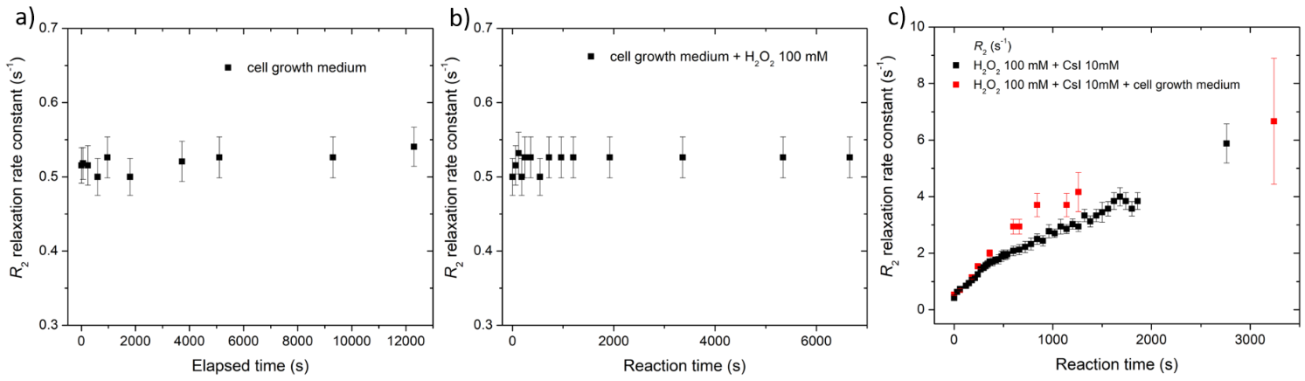

Fig. S7. Cell growth medium stability (a), monitoring after addition of 100 mM H_2O_2 (b), addition of 10 mM CsI (c)

The stable R_2 values shown in Fig. S7 (b) indicate that any chemical reactions between the hydrogen peroxide in this medium in the absence of CsI does not yield PRE-generating compounds. A high concentration of H_2O_2 was employed (100 mM) in order to readily detect any possible interference with the formation of paramagnetic O_2 due to the oxidation of compounds in the cell-growth medium. Subsequently, 50 mM CsI was added to catalyze H_2O_2 decay and the R_2 data is shown in Fig. S7. (c). A time-dependent increase of R_2 was readily detected. The data is compared to the equivalent experiment without any cell-growth medium presented in the article. The detected profiles are similar, with slightly increased R_2 values for water ^1H in the cell-growth medium, which most likely stem from the increased effective correlation times for relaxation mechanisms in this medium due to sample viscosity.

IV. Comparison between different magnetic resonance methods for the detection of free-radicals in water

The generation of paramagnetic species in water can be detected directly using electron spin resonance (ESR) and indirectly by nuclear magnetic resonance (NMR). The incentive for NMR detection, as discussed in the main text, are advantages in terms of spatial resolution for imaging applications afforded by the lifetimes of nuclear spin magnetisation, which enables the use of long field gradients. Paramagnetic effects on water protons can be detected via NMR chemical shift dispersion[1] or via NMR relaxation.[2-4] Measuring chemical shifts requires highly-homogeneous magnetic fields provided by high-resolution NMR spectrometers, which are expensive devices due to the fact that superconducting magnets are used. Moreover, the susceptibility-induced field distortions generated in many applications of interest involving paramagnetic species can render the use of high-resolution NMR extremely difficult for free radicals. A more straightforward approach is the use of time-domain NMR relaxation, which can be detected at any field strength and even in inhomogeneous fields.[5] Time-domain relaxation methods can be deployed on a wide range of NMR equipment, such as benchtop and portable/mobile instruments, typically operating at low-fields. The main advantages of using NMR in Earth's field are primarily the long signal life time and the very low cost of the equipment.

Table S4. Comparison of the characteristics of magnetic resonance experimental devices amenable to free-radical detection.

Method	^{1}H frequency	Spatial imaging capability	Pros	Cons
Earth-Field NMR (EF-NMR)	2.3 kHz	Yes	-Highly homogeneous field; -Long signal lifetime; -Portable; -Easy access to sample, open-top/bottom; - Low cost - Circumvents the use of additional static magnetic fields during detection	-Large sample volumes -Low sensitivity
Portable/mobile Low-Field NMR (LF-NMR)	Tens of MHz	Yes	- Portable - Small sample volumes (mL)	-Inhomogeneous field
Benchtop LFNMR	Up to 100 MHz	Limited	-Fairly homogeneous field -Fair sensitivity	- Less portable or not portable
High-Field NMR (HF-NMR)	Above 100 MHz	Yes	- Homogeneous field - Most sensitive	- Expensive -Lab environment only

Water relaxation in the presence of paramagnetic species was widely studied in the field of biochemistry, chemical engineering and medical imaging.[4,6] Redox reactions and complexation were for the first time followed by NMR relaxometry in 1973.[7] Decomposition of hydrogen peroxide in catalytic reactions was investigated by relaxometry at low- and high-field NMR and in combination with pH measurements allowed the determination of its concentration during the reaction.[8] Time-domain relaxometry was successfully employed to determine concentrations of paramagnetic metal cations in aqueous solutions.[4,9,10] Earth-field NMR detection is adapted for applications where magnetic fields would interfere with the detected effect, such as radiobiology with charged particle beams[11]. To our knowledge, this article shows

the first demonstration of Earth-field NMR relaxation detection of paramagnetic effects induced by free-radicals generated *in situ*.

References:

1. A. J. Pell, G. Pintacuda, C. P. Grey, *Prog. Nucl. Magn. Reson.*, 2019, **111**, 1–271.
2. G. Chiarotti, G. Cristiani, L. Giulotto, *Nuovo Cim*, **1955**, *1* (5), 863–873.
3. D. S. Parker, J. F. Harmon, *Chem. Phys. Lett.* 1974, **25 (4)**, 505–506.
4. F. Kock, L. Colnago, *J. Braz. Chem. Soc.*, 2022.
5. B. Blümich, *J. Magn. Reson.*, 2019, **306**, 27–35.
6. C. Luchinat, *Magn. Reson. Chem.*, 1993, **31 (13)**, S145–S153.
7. A. Schluter, A. Weiss, *Z. Anal. Chem.* 1973, **266 (3)**, 177–186.
8. L. Buljubasich, B. Blümich, S. Stapf, *Chem. Eng. Sci.* 2010, **65 (4)**, 1394–1399.
9. B. F. Gomes, J. S. da S. Burato, C. M. Silva Lobo, L. A. Colnago, *Int. J. Anal. Chem.*, 2016, **2016,** 1–5.
10. Y. Gossuin, P. Duez, B. Blankert, C. Masson, S. Laurent, C. Rousseau, *Magn. Reson. Chem.* 2023, **61 (5)**, 284–295.
11. H. Fuchs, F. Padilla-Cabal, L. Zimmermann, H. Palmans, D. Georg, Med. Phys. 2021, 48(5): 2572–2579